Electronic Supplementary Material (ESI) for Materials Horizons.

Supporting Information

Anti-Correlation Effect of Alkyl Chain Size on Photovoltaic Performance in Centrally Extended Non-Fullerene Acceptors

Tainan Duan, Jia Wang, Xiaochan Zuo, Xingqi Bi, Cheng Zhong, Yulu Li, Yuhong Long, Kaihuai Tu, Weichao Zhang, Ke Yang, Huiqiong Zhou, Xiangjian Wan, Yan Zhao, Bin Kan, and Yongsheng Chen

Content:

1. Materials and Methods

All reactions were performed under nitrogen atmosphere and solvents were purified and dried from appropriate drying agents using standard techniques prior to use. Polymer donor **PM6**, 2-(5,6-difluoro-3-oxo-2,3-dihydro-1H-inden-1-ylidene)malononitrile (**INCN-2F**) and acceptor **BO-4Cl** were purchased from Organtec. Ltd, Woerjiming (Beijing) Technology Development Institute and Seniormaterial (Wuxi), respectively. Reagents available from commercial sources were used without further purification unless otherwise stated.

All unreported compounds were characterized by NMR spectroscopy on Bruker Avance III Ultrashield Plus instruments (600 MHz). High-resolution mass spectrometry (HR-MS) data of new acceptors were recorded using a Bruker solariX XR platform.

2. Synthetic Protocols and Characterizations

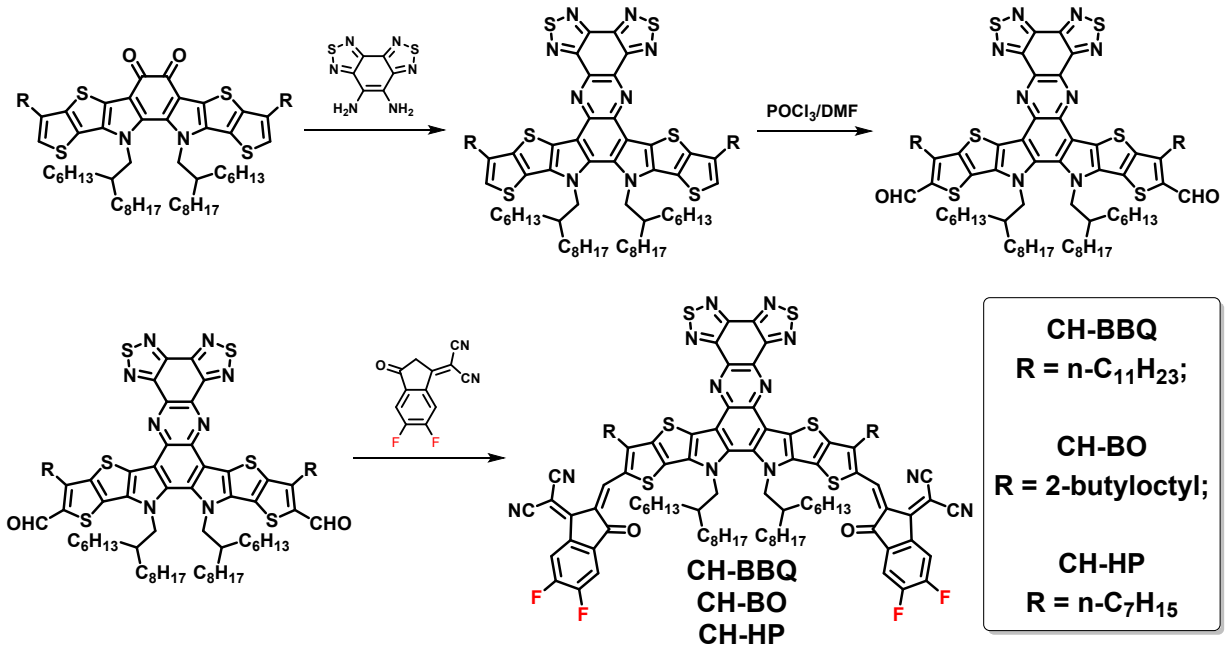

Figure S1. Synthetic route of the non-fullerene acceptors.

General procedure for the preparation of CH-series acceptors: CH-BO and **CH-HP** were synthesized as same as we prepared **CH-BBQ** in our previous work.[1]

CH-BO: Deep purple solid (98 mg, 81%). ^{1}H NMR (600 MHz, $CHCl_3$, δ ppm): 9.11 (s, 2H), 8.43-8.41 (m, 2H), 7.75-7.73 (m, 2H), 4.94 (d, J = 7.2 Hz, 4H), 3.26 (d, J = 7.2 Hz, 4H), 2.33 (br, 2H), 2.12 (br, 2H), 1.51-0.85(m, 92H), 0.74-0.70 (m, 12H). ^{13}C NMR (151 MHz, $CDCl_3$, δ ppm): 186.06, 158.82, 155.30, 155.21, 154.62, 153.73, 153.55, 153.46, 149.08, 146.90, 138.24, 137.32, 137.24, 136.57, 135.59, 135.49, 134.58, 134.21, 134.04, 131.15, 120.16, 119.15, 115.06, 115.00, 114.86, 114.40, 112.47, 112.35, 68.63, 56.02, 40.27, 39.47, 34.74, 33.75, 33.46, 31.97, 31.88, 31.63, 30.71, 30.67, 29.89, 29.66, 29.56, 29.42, 29.22, 29.05, 26.75, 25.81, 25.74, 23.06, 22.69, 22.61, 22.49, 14.27, 14.16, 14.04. HR-MS [m/z]: calcd. for $C_{106}H_{123}F_4N_{12}O_2S_6^+$ $[M+H]^+$ 1863.8147, found 1863.8102.

CH-HP: Purple-brown solid (105 mg, 81%). ^{1}H NMR (600 MHz, $CHCl_3$, δ ppm): 9.09 (s, 2H), 8.45-8.43 (m, 2H), 7.77-7.75 (m, 2H), 4.96 (d, J = 7.2 Hz, 4H), 3.28 (br, 4H), 2.35 (br, 2H), 1.88 (br, 2H), 1.58 (br, 4H), 1.40-0.90 (m, 66H), 0.73-0.70 (m, 12H). ^{13}C NMR (151 MHz, $CDCl_3$, δ

ppm): 186.11, 158.45, 155.31, 155.22, 154.31, 154.02, 153.58, 153.49, 148.88, 146.60, 138.27, 137.02, 136.96, 136.55, 135.71, 135.12, 134.48, 134.06, 133.36, 131.07, 119.98, 119.10, 114.97, 114.86, 114.40, 112.58, 112.46, 68.70, 56.04, 39.58, 31.87, 31.76, 31.71, 30.82, 30.78, 29.99, 29.89, 29.86, 29.67, 29.50, 29.28, 29.24, 25.97, 25.91, 22.75, 22.59, 22.52, 14.15, 14.05, 14.03. HR-MS [m/z]: calcd. for $C_{96}H_{103}F_4N_{12}O_2S_6^+$ $[M+H]^+$ 1723.6582, found 1723.6547.

3. Cyclic Voltammogram

Electrochemical measurements were performed with a LK98B II Microcomputer-based Electrochemical Analyzer, using a glassy carbon button electrode as the working electrode, a platinum wire as the auxiliary electrode, and a saturated calomel electrode (SCE) as the reference electrode. Tetrabutyl ammonium phosphorus hexafluoride (n-Bu_4NPF_6, 0.1 M) in acetonitrile was employed as the electrolyte, and the scan rate was set to be 100 mV s^{-1}. The SCE was calibrated using the ferrocene/ferrocenium (Fc/Fc^+) redox couple. Fc/Fc^+ is taken to be 4.8 eV relative to the vacuum level. [2]

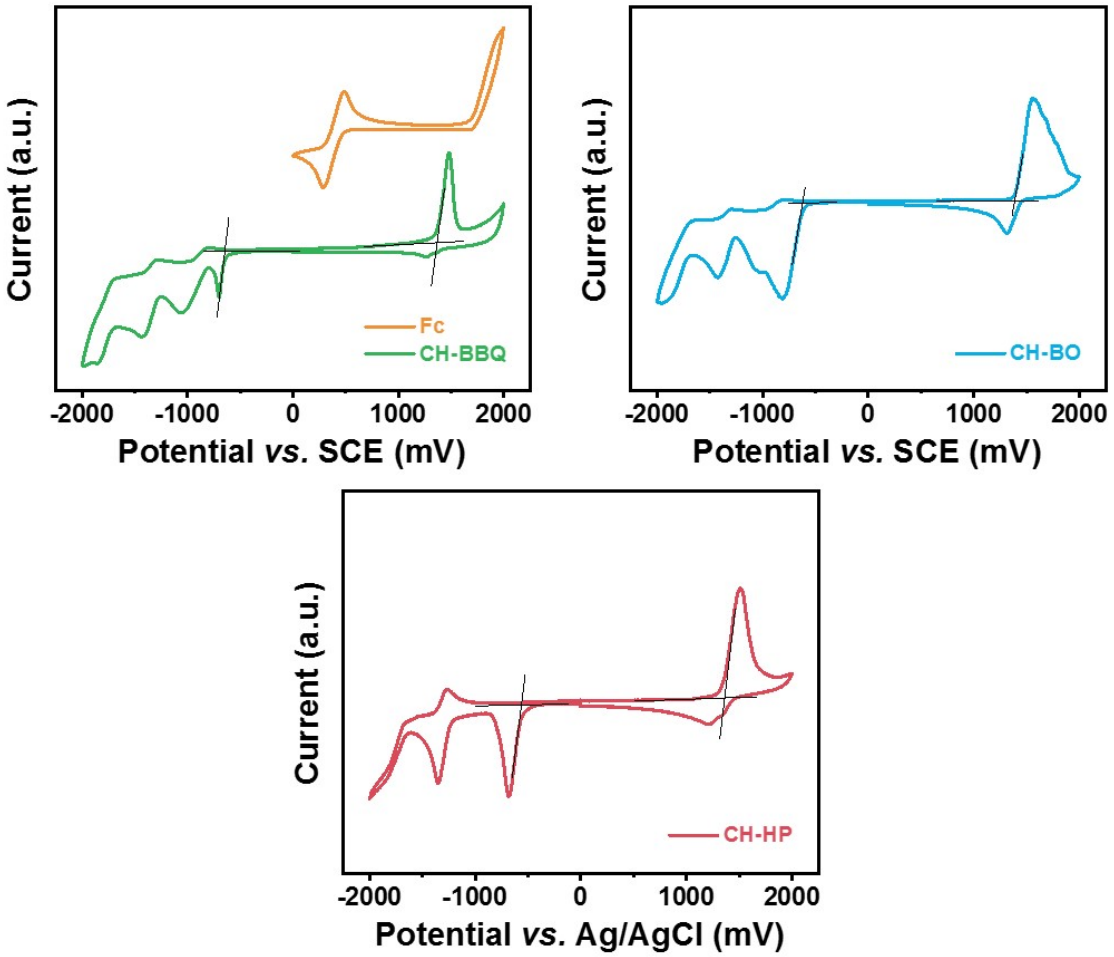

Figure S2. Oxidation/reduction scans of the acceptors along with ferrocene.

4. UV-Vis Spectroscopy

UV-Vis spectra in solution/film were recorded on a Cary 5000 UV-Vis spectrophotometer. The concentration of diluted solutions of acceptor was *ca.* 10^{-5} M. And the concentration of the solution for preparing the thin film of acceptor was *ca.* 15 mg mL^{-1}.

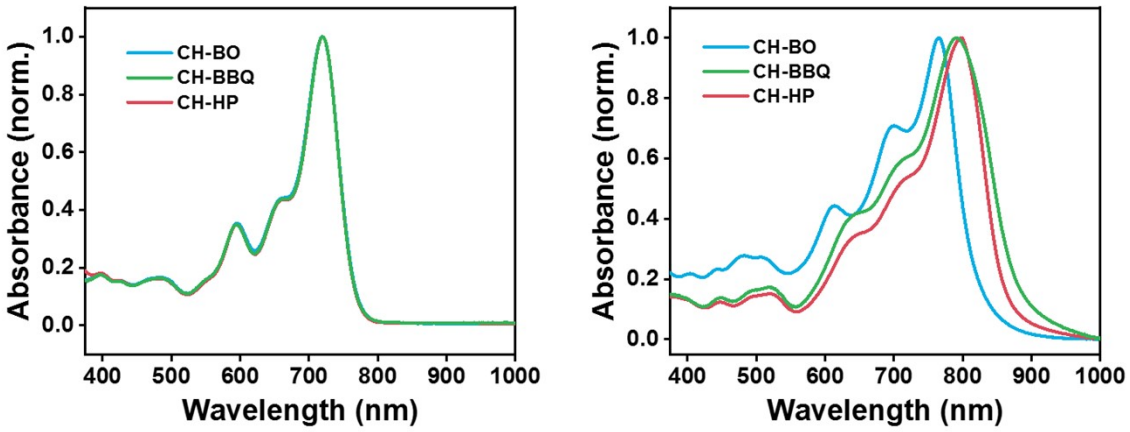

Figure S3. Normalized UV-vis spectra of acceptors in **(left)** chloroform solution and **(right)** in film.

Table S1. The photophysical and electrochemical properties of acceptors.

Molecule	λsol max (nm)	λfilm max nm)	Δλ (nm)	λfilm onset (nm)	Eox onset (V)	Ered onset (V)	Eopt gap[a] (eV)	LUMO[b] (eV)	HOMO[b] (eV)
CH-BO	720	765	**45**	821	1.39	-0.63	1.51	-3.85	-5.87
CH-BBQ	720	791	71	874	1.36	-0.56	1.44	-3.92	-5.84
CH-HP	720	799	**79**	858	1.37	-0.64	1.42	-3.84	-5.85

[a] Eopt gap is derived from the absorption onset of the neat film of donor/acceptor: Eopt gap = 1240/λfilm onset;

[b] E_{HOMO} = -[Eox onset + (4.8 – $E_{Fc/Fc+}$)] eV; E_{LUMO} = -[Ered onset + (4.8 – $E_{Fc/Fc+}$)] eV.

5. In-situ UV-vis absorption spectra

The in-situ UV-vis absorption spectra was recorded during spin-coating process by using OEM-LUMETTA CCD (Horiba Jobin-Yvon Inc.). The light source is halogen lamp (Model HL1000, Wyoptics). The exposed time of every test was 0.25s.

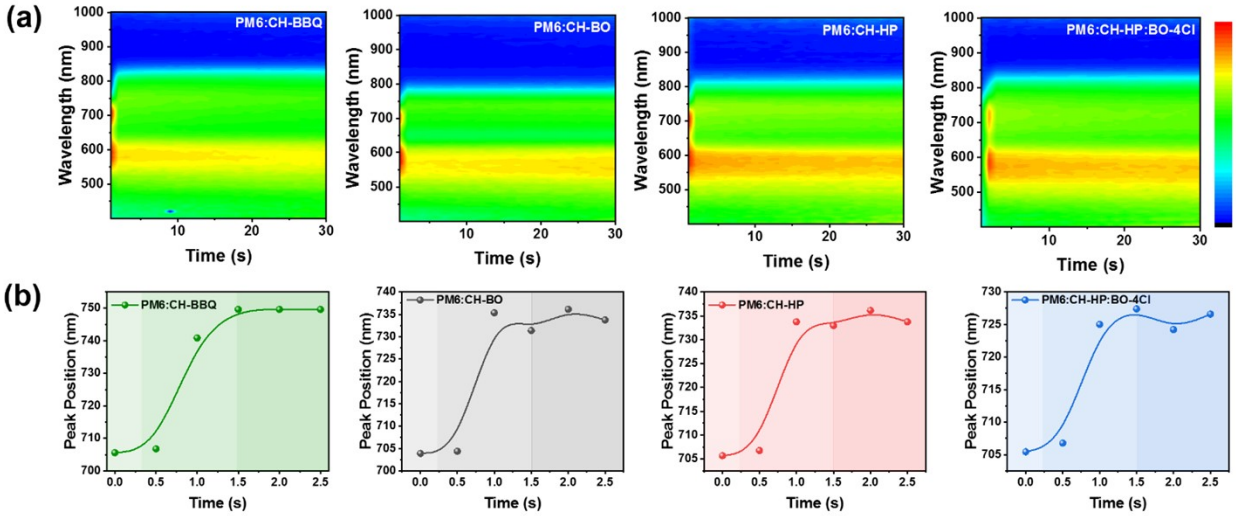

Figure S4. (a) The color mapping of in situ UV-vis reflectance spectra as a function of spin-coating time. (b) In situ absorption location as a function of spin-coating time.

6. Photoluminescence (PL) spectroscopy

The PL spectra of neat films and blend films were measured by using FLS1000 spectrometer.

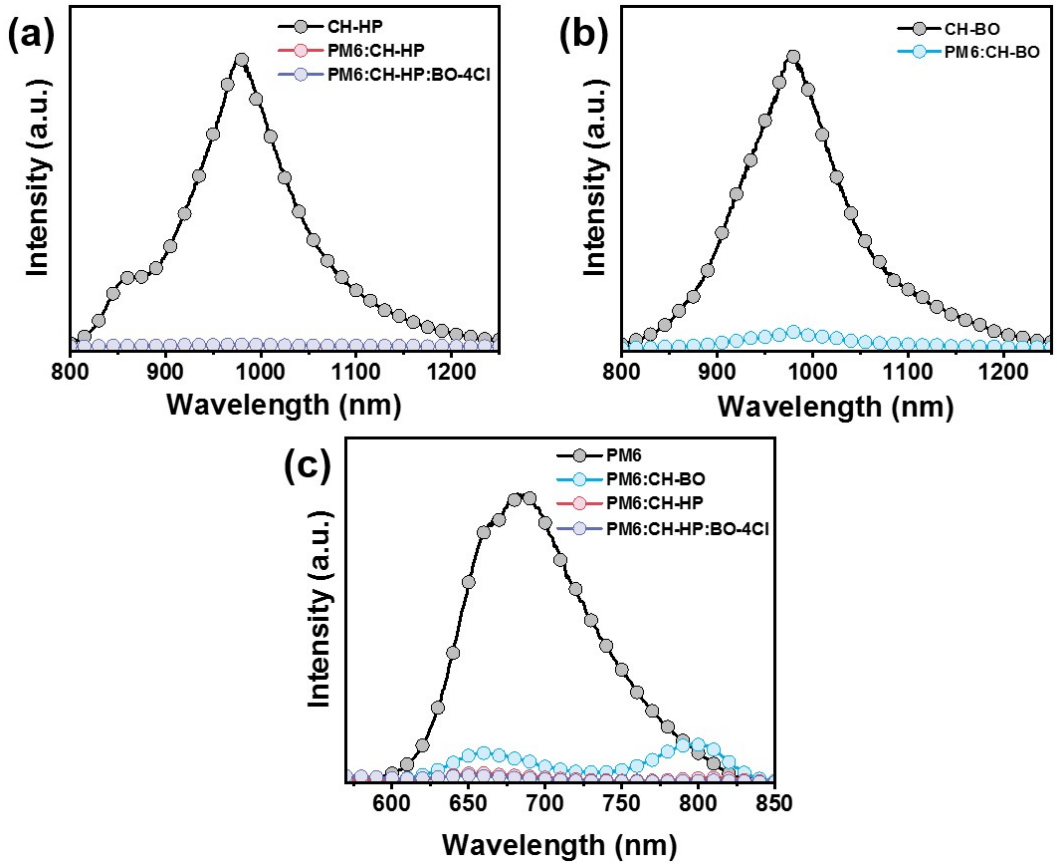

Figure S5. (a, b) The PL spectra of neat films and blend films excited by a wavelength of 761 and 690 nm, respectively. (c) The PL spectra of neat films and blend films excited by a wavelength of 469 nm.

Table S2. The PL parameters of neat films and blend films.

Film	λ_{ex} (nm)	λ_{em} (nm)	Quenching Efficiency (%)
PM6	469	682	\
PM6:CH-BO		658, 796	89.7
PM6:CH-HP		654, 811	96.7
PM6:CH-HP:BO-4Cl		655, 815	97.5

Film	λ_{ex} (nm)	λ_{em} (nm)	Quenching Efficiency (%)
CH-BO	761	976	\
PM6:CH-BO		980	93.5
CH-HP	690	975	\
PM6:CH-HP		979	97.8
PM6:CH-HP:BO-4Cl		972	97.7

7. Thermogravimetry Analysis (TGA)

The TGA of NFAs was conducted on a NETZSCH STA 49 409PC instrument under nitrogen atmosphere using aluminum crucibles. The heating rate is 10 °C/min.

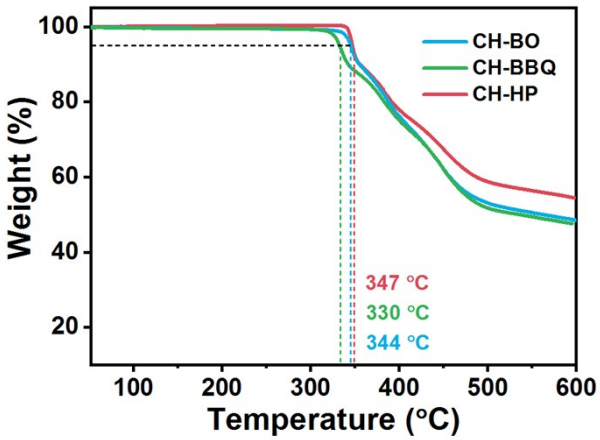

Figure S6. TGA curves of NFAs. All three acceptors show good thermal-stability; *ca.* 5% weight loss observed at 344, 330 and 347 °C for CH-BO, CH-BBQ and CH-HP, respectively.

8. Urbach Energy Measurements

The Urbach energy (E_u) of sole acceptor based devices was evaluated by measuring the fourier transform photocurrent spectroscopy-external quantum efficiency (FTPS-EQE).

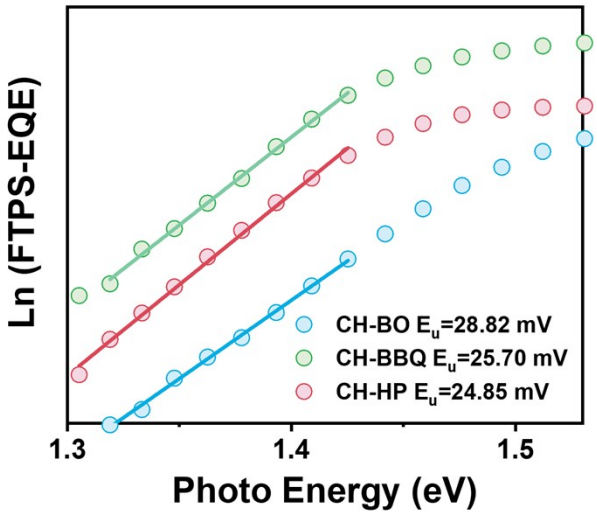

Figure S7. Urbach energy of sole acceptor based devices.

9. Crystal data and structure refinement for CH-BO and CH-HP

Table S3. Crystallographic parameters of CH-BO and CH-HP.

	CH-HP	**CH-BO**
Empirical formula	$C_{96}H_{102}F_4N_{12}O_2S_6$	$C_{106}H_{122}F_4N_{12}O_2S_6$
Formula weight	1724.25	1864.51
Temperature/K	150	193.00
Crystal system	monoclinic	monoclinic
Space group	P 2_1/n	C 2/c
a/Å	20.6737(13)	25.733(2)
b/Å	21.4410(15)	25.060(2)
c/Å	25.9830(19)	20.5893(16)
α/°	90	90
β/°	107.449(4)	107.794(3)
γ/°	90	90
Volume/Å^3	10987.4(13)	12642.1(18)
Z	4	4
ρ_{calc}g/cm^3	1.042	0.980
μ/mm^{-1}	1.572	0.913
F(000)	3640.0	3960.0

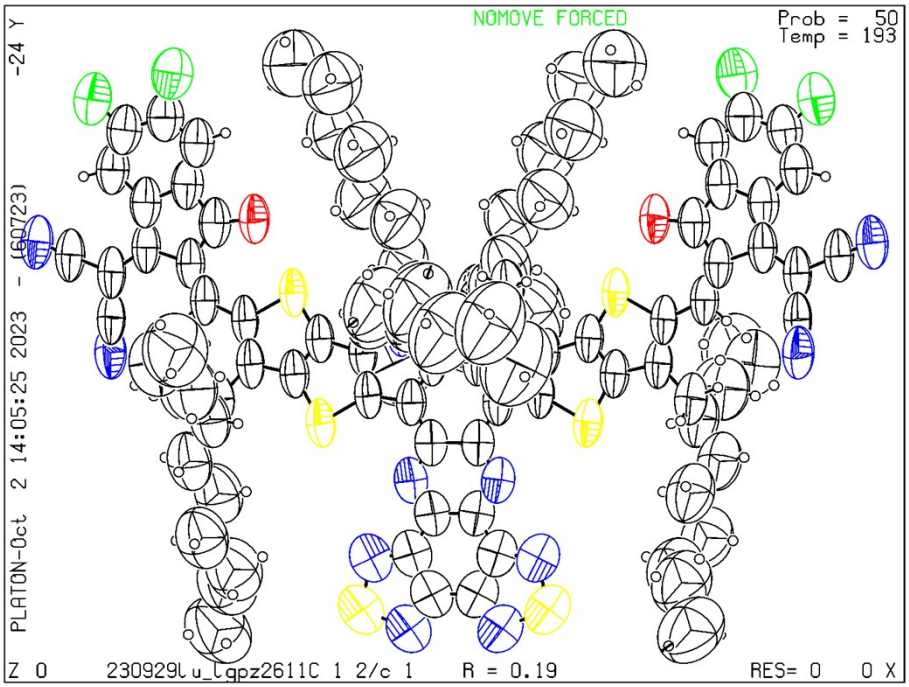

Figure S8. The ORTEP illustration with probability ellipsoids of CH-BO (CCDC No. 2300122).

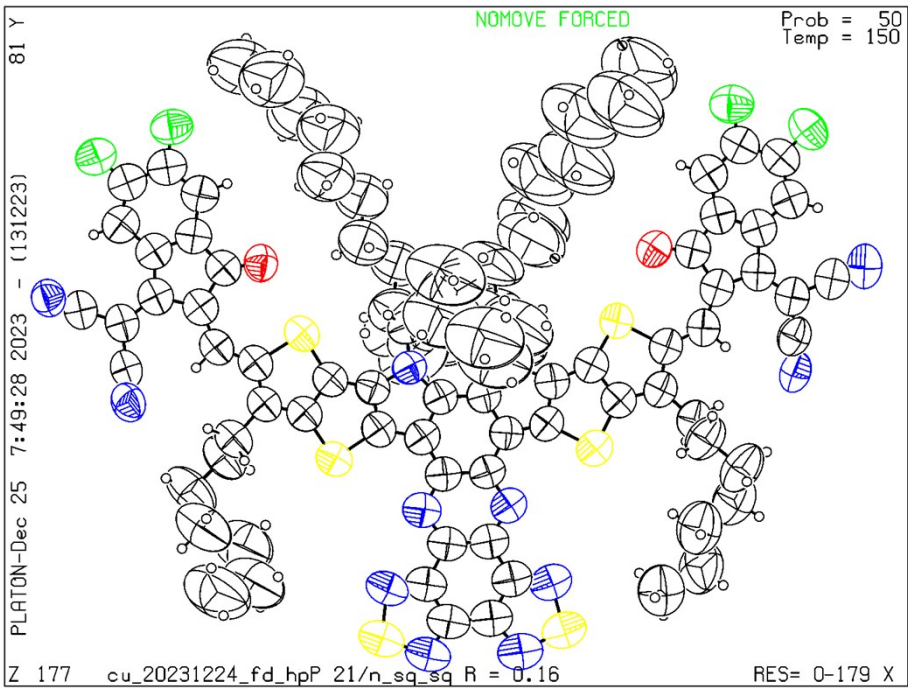

Figure S9. The ORTEP illustration with probability ellipsoids of CH-HP (CCDC No. 2321689).

10. Device Fabrication and Characterizations

OFET devices

The bottom-gate top-contact (BGTC) devices based on the single-crystals of CH-BO and CH-HP growing on the SiO_2/Si substrates were fabricated with the "gold strips" method to investigate charge transport properties. The SiO_2/Si wafers used to grow crystals were first cleaned with hot piranha solution (H_2SO_4/H_2O_2 = 2:1) followed by a copious rinsing with deionized water and finally were blown dry by nitrogen gun. Single crystals of CH-BO and CH-HP were synthesized via drop-casting their chlorobenzene solution (0.2 mg/mL) and chloroform solution (0.1 mg/mL), respectively, onto SiO_2/Si substrates in a sealed bottle under typical growth conditions at room temperature. The solvent was controlled to slowly evaporate in several days. Then the single crystals in micrometer scale may grow on the substrates. The best quality crystals were selected on a micromanipulator station coupled with an optical microscope to further fabricate the transistor devices. Two pieces of the Au films, approximately 150 μm × 30 μm, were glued onto the selected single crystals via the electrostatic forces with the help of the S8mechanical probes in the Micromanipulator. The abovementioned Au films were prepared as follow: firstly, a patterned Au thin film with a thickness around 100 nm was predeposited on a Si wafer by thermal evaporation with a copper mask. Then, two small pieces of the Au films with desired sizes were peeled off from the Si substrate with the tip of the mechanical probe and transferred onto the single crystals as source and drain electrodes. The Si substrate functioned as the gate electrode.

The electrical properties of OFETs were measured using a semiconductor parameter analyzer (Platform Design Automation FS380 Pro) in glove box with nitrogen atmosphere. The charge mobility was extracted from the saturation regime and calculated from the following equation:

$$I_{DS} = \frac{W}{2L} C_i \mu \left(V_{GS} - V_T\right)^2$$

Where I_{DS} is the drain-source current, μ is the field-effect mobility W/L is the channel width/length, C_i is the capacitance per unit area of gate dielectric layer, and V_G and V_T are the gate voltage and threshold voltage, respectively.

OSC devices

The conventional devices based on PM6:Acceptors were fabricated with an architecture of ITO/PEDOT:PSS(4083)/PM6:ACCEPTOR/PNDIT-F3N[3]/Ag. Firstly, the ITO glass was pre-cleaned sequentially in an ultrasonic bath of detergent, deionized water, acetone and isopropanol. Then the surface of ITO was treated by UV light in an ultraviolet-ozone chamber (Jelight Company) for 15min. Afterwards, a thin layer of poly(3,4-ethylene dioxythiophene):poly(styrene sulfonate) (PEDOT:PSS, 95 Baytron PVP Al 4083) was prepared by spin-coating the PEDOT:PSS solution at 4400 rpm for 20s on the ITO substrate. Subsequently, the PEDOT:PSS films were baked at 160 °C for 15 min in air and transferred to a argon-filled glove box. Then the PM6:CH-BO or PM6:CH-HP or PM6:CH-HP:BO-4Cl mixtures were fully dissolved in chloroform (CF) with 2,5-dichloro-3,4-diiodothiophene (CIT) as solid additive (PM6 concentration of 6 mg mL^{-1}). In addition, 0.15 % v/v 1-chloronaphthalene(1-CN) as the second additive were added in PM6:CH-HP and PM6:CH-HP:BO-4Cl systems. The resulting solutions were spin-casted onto the PEDOT:PSS layer at 2000 rpm for 25s. Then the films were treated with the thermal annealing (TA). The optimized active layer thickness is about 105 nm. After that, a thin layer of PNDIT-F3N (dissolved in methanol in concentration of 1 mg/mL) was spin-coated on the top of the active layer. Finally, a layer of Ag with thickness of 150 nm was deposited under 2×10^{-6} Pa. The active area of the device was *ca.* 4 mm^2, and a shadow mask with defined area of 3.24 mm^2 was used during the testing. The current density-voltage (*J*-V) curves of the prepared photovoltaic devices were recorded by a Keithley 2400 source-measure unit. The photocurrent was measured under the simulated illumination of 100 mW cm^{-2} with AM1.5 G using a Enli SS-F5-3A solar simulator, which was calibrated by a standard Si solar cell (made by Enli Technology Co., Ltd., Taiwan, and calibrated report can be traced to NREL). The thickness of the active layers was measured by a Veeco Dektak 150 profilometer. The EQE spectra were recorded by using a QE-R Solar Cell. Response Measurement System (Enli Technology Co., Ltd., Taiwan).

11. Additional OSC device data

Table S4. Device optimization of **PM6:CH-BO** based binary devices.

D:A ratio (m/m)	Weight ratio of CIT to D	Post-treatment	V_{OC} (V)	J_{SC} (mA cm^{-2})	FF (%)	PCE (%)
1:0.8	\	\	0.999	17.52	59.6	10.43
1:1	\	\	0.997	17.06	59.4	10.11
1:1.2	\	\	0.999	16.06	57.0	9.14
1:0.8	80%	90 °C 8 mins	0.983	17.78	64.1	11.24
	90%		0.983	17.86	63.8	11.24
	100%		0.964	17.78	61.8	10.63
	110%		0.964	18.58	63.0	11.32
	110%	80 °C 8 mins	0.960	17.27	64.3	10.58
		90 °C 8 mins	0.964	18.58	63.0	11.32
		100 °C 8 mins	0.984	17.46	66.9	11.43

Table S5. Device optimization of **PM6:CH-HP** based binary devices.

D:A ratio (m/m)	Weight ratio of CIT to D	CN (v/v)	Post-treatment	V_{OC} (V)	J_{SC} (mA cm^{-2})	FF (%)	PCE (%)
1:0.8	\	\	\	0.929	23.33	72.9	15.79
1:1	\	\	\	0.924	24.42	73.9	16.70
1:1.2	\	\		0.920	24.98	71.9	16.54
1:1.4	\	\	\	0.907	25.43	68.8	15.87
1:1.1	70%	\	90 °C 8 mins	0.899	25.63	78.1	17.99
	80%	\		0.897	26.27	77.6	18.37
	90%	\		0.891	26.32	77.9	18.33
	100%	\		0.892	26.04	78.5	18.30
	80%	\	80 °C 8 mins	0.898	25.80	78.5	18.19
		\	90 °C 8 mins	0.897	26.27	77.6	18.37
		\	100 °C 8 mins	0.894	25.65	78.9	18.10
		0.05%	90 °C 8 mins	0.897	26.14	77.4	18.08
		0.15%		0.903	25.89	80.1	18.74
		0.25%		0.888	25.30	77.9	17.51

Table S6. Device optimization of **PM6:CH-HP:BO-4Cl** based ternary devices.

D:A ratio (m/m)	Weight ratio of CIT to D	CN (v/v)	Post-treatment	V_{OC} (V)	J_{SC} (mA cm^{-2})	FF (%)	PCE (%)
1:0.9:0.2	**80%**	**0.15%**	**90 °C 8 mins**	**0.893**	**26.83**	**78.6**	**18.83**
1:0.8:0.4				**0.885**	**27.97**	**78.5**	**19.44**

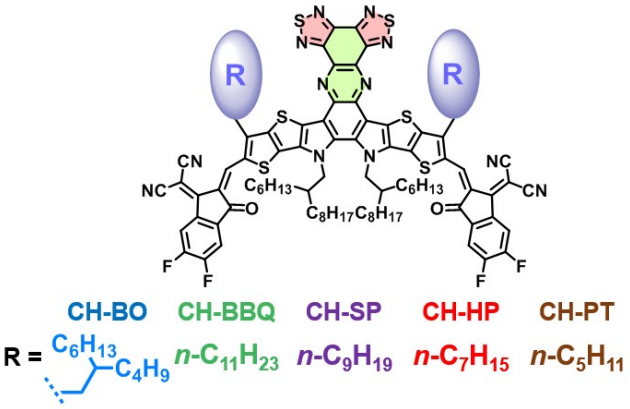

Figure S10. The chemical structures of CH-BBQ derived acceptors with different side chains.

Table S7. The PV parameters of as cast devices based CH-BBQ (C11), CH-NY (C9), CH-HP (C7) and CH-PT (C5).

D:A	D:A ratio (m/m)	Post-treatment	V_{OC} (V)	J_{SC} (mA cm^{-2})	FF (%)	PCE (%)
PM6:CH-PT	1:1.1	90 °C, 8 mins	0.891	24.25	71.8	15.46
PM6:CH-HP			0.909	25.33	76.6	17.59
PM6:CH-NY			0.908	25.44	74.8	17.21
PM6:CH-BBQ			0.914	24.62	76.0	17.05

12. E_{loss} Analysis

The following equation was used to quantify the E_{loss} of OSCs:

$$E_{\text{loss}} = E_{\text{g}}^{\text{PV}} - qV_{\text{oc}} = \left(E_{\text{g}}^{\text{PV}} - qV_{\text{oc}}^{\text{SQ}}\right) + \left(qV_{\text{oc}}^{\text{SQ}} - qV_{\text{oc}}^{\text{rad}}\right) + \left(qV_{\text{oc}}^{\text{rad}} - qV_{\text{oc}}\right) = \Delta E_1 + \Delta E_2 + \Delta E_3$$

*E*PV g represents the bandgap of the blend film and *q* is the elementary charge. *E*PV g can be estimated via the derivatives of the sensitive EQE (EQE_{PV}) spectra(P(E)=*d*EQE/*d*E) as following:

$$E_{\text{g}}^{\text{PV}} = \frac{\int_a^b E_{\text{g}} \text{P}(E_{\text{g}}) \text{d}E_{\text{g}}}{\int_a^b \text{P}(E_{\text{g}}) \text{d}E_{\text{g}}}$$

where the integration limits *a* and *b* are chosen as the energy where P(E_g) is equal to 50% of its maximum, as exemplarily depicted in **Figure S11**. The EQE_{PV} measurements were conducted on an Enlitech FTPS PECT-600 instrument. The total E_{loss} can be divided into three parts:

(1) $\Delta E_1 = E_g - qV_{\text{oc}}^{\text{SQ}}$ represents the unavoidable radiative loss originating from absorption above the bandgap. The $V_{\text{oc}}^{\text{SQ}}$ is the maximum voltage based on the Shockley–Queisser (SQ) limit:

$$V_{\text{oc}}^{\text{SQ}} = \frac{kT}{q} \ln\left(\frac{J_{\text{sc}}^{\text{SQ}}}{J_0^{\text{SQ}}} + 1\right) \cong \frac{kT}{q} \ln\left(\frac{q \cdot \int_{E_{\text{g}}}^{+\infty} \phi_{\text{AM1.5G}}(E) \text{d}E}{q \cdot \int_{E_{\text{g}}}^{+\infty} \phi_{\text{BB}}(E) \text{d}E}\right)$$

(2) $\Delta E_2 = qV_{\text{oc}}^{\text{SQ}} - qV_{\text{oc}}^{\text{rad}}$ can be regarded as radiative loss caused by absorption below the bandgap, where the $V_{\text{oc}}^{\text{rad}}$ is the open circuit voltage when there is only radiative recombination. The radiative recombination limit for the saturation current (J_0^{rad}) is also calculated from the EQE spectrum:

$$V_{oc}^{rad} = \frac{kT}{q}\ln\left(\frac{J_{sc}}{J_0^{rad}}+1\right) \cong \frac{kT}{q}\ln\left(\frac{q\cdot\int_0^{+\infty}\mathrm{EQE}(E)\phi_{AM1.5G}(E)\mathrm{d}E}{q\cdot\int_0^{+\infty}\mathrm{EQE}(E)\phi_{BB}(E)\mathrm{d}E}\right)$$

where q is the elementary charge and ϕ_{BB} is the black body spectrum at 300 K.

(3) $\Delta E_3 = qV_{oc}^{rad} - qV_{oc}$ can be directly calculated while the other two parts were determined. ΔE_3 can also be confirmed by measuring the EQE of electroluminescence (EQE_{EL}) of the solar cell through the equation of: $\Delta E_3 = -kT\ln(EQE_{EL})$. For the EQE_{EL} measurements, a digital source meter (Keithley 2400) was 80 employed to inject electric current into the solar cells, and the emitted photons were collected by a Si diode (Hamamatsu s1337-1010BQ) and indicated by a picoammeter (Keithley 6482).

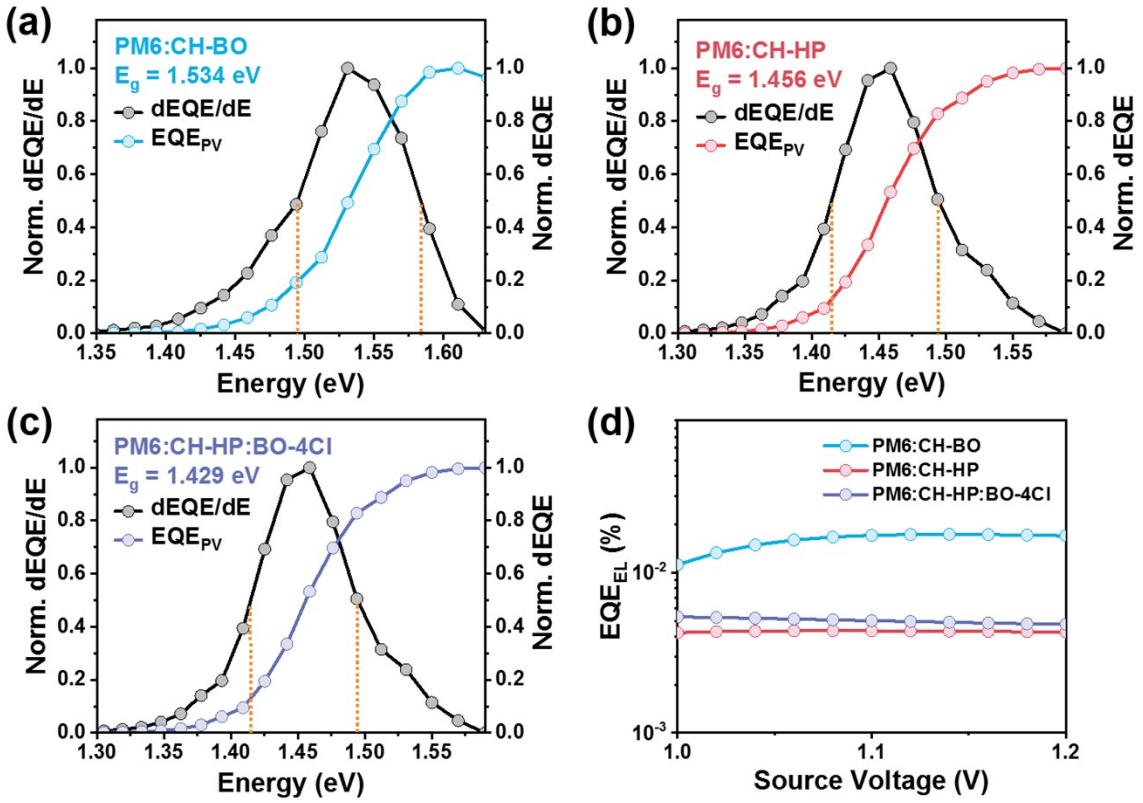

Figure S11. (a-c) Optical bandgap determination of blend films on the basis of the derivatives of the sensitive EQE spectra for optimized OSCs. (d) EQE_{EL} spectra for the binary and ternary devices.

Table S8. Detailed distributions of total energy loss in OSCs based on the SQ limit theory.

Blend	EPV g (eV)	VSQ OC (V)	ΔE_1 (eV)	Jrad 0 (10^{-17} A/m²)	Vrad OC (V)	ΔE_2 (eV)
PM6:CH-BO	1.534	1.260	0.274	0.207	1.122	0.078
PM6:CH-HP	1.456	1.188	0.268	1.760	1.078	0.050
PM6:CH-HP:BO-4Cl	1.429	1.163	0.266	6.170	1.047	0.057

Blend	ΔE_3 (eV)[a]	EQE_{EL} (10^{-4})	ΔE_3 (eV)[b]	V_{oc} (V)	E_{loss} (eV)
PM6:CH-BO	0.206	1.49	0.227	0.976	0.559
PM6:CH-HP	0.239	0.39	0.262	0.899	0.557
PM6:CH-HP:BO-4Cl	0.223	0.53	0.254	0.883	0.546

[a] Calculated from the VSQ OC through the equation of: $\Delta E_3 = qV\text{rad OC} - qV_{OC}$;

[b] Calculated from the EQE_{EL} through the equation of: $\Delta E_3 = -kT\ln(EQE_{EL})$.

13. Charge Carrier Mobility Measurements

The carrier mobility (hole and electron mobility) of photoactive active layer was obtained by fitting the dark current of hole/electron-only diodes to the space-charge-limited current (SCLC) model. Hole-only diode configuration: Glass/ITO/PEDOT:PSS/active layer/MoO_3/Ag; Electron-only diode configuration: Glass/ITO/ZnO/active layer/PNDIT-F3N/Ag. The SCLC mobility was estimated using the following equation:

$$J = \frac{9\varepsilon_r\varepsilon_0\mu V^2}{8L^3}$$

where J is the current density, ε_r is the dielectric permittivity of the active layer, ε_0 is the vacuum permittivity, L is the thickness of the active layer, μ is the hole/electron mobility.

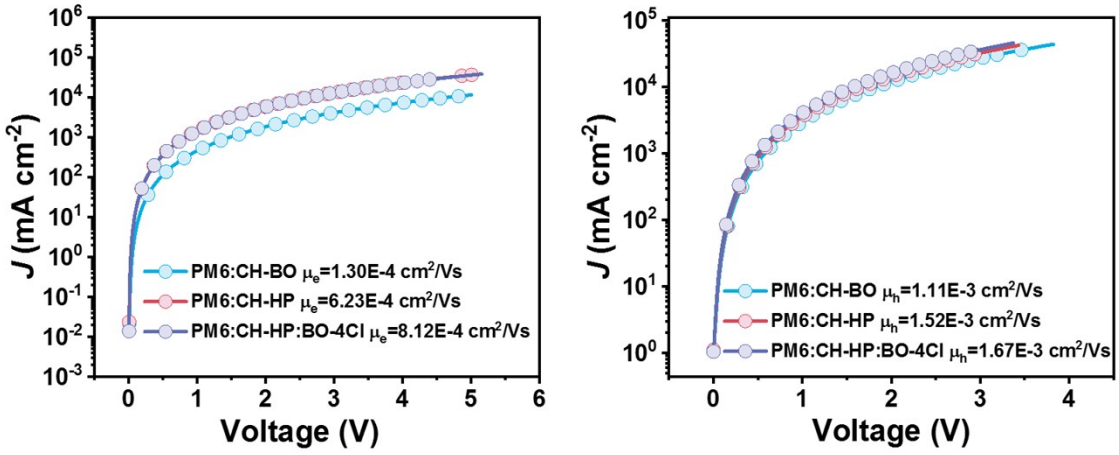

Figure S12. (a) electron and (b) hole mobility of BHJs under the optimized condition

Table S9. Average mobility values of optimized devices.

Molecule	μ_e ($\times10^{-4}$ cm^2/Vs)	μ_h ($\times10^{-4}$ cm^2/Vs)	μ_h/μ_e
PM6:CH-BO	1.30	11.1	8.54
PM6:CH-HP	6.23	15.2	2.43
PM6:CH-HP:BO-4Cl	8.12	16.7	2.06

14. Charge Carrier Recombination Analysis

In OSCs, bimolecular recombination and trap-assisted recombination are the two major charge carrier recombination channels that would results the loss of PCEs. To probe how these recombination losses affect the device performances, *J*–*V* characteristics under different light intensities were measured. To quantify the bimolecular recombination rate, the relationship between J_{SC} and light intensity was investigated. According to previous reports, J_{SC} and incident light intensity (I) show a power-law dependence of $J \propto I^{\alpha}$, where α represents the power factor. The bimolecular recombination efficiency (η) then can be quantified as $\eta = 1/\alpha - 1$, which means the closer the α is to 1, the more unlikely bimolecular recombination occurs. Similarly, the trap-assisted recombination can be recorded by monitoring the relationship between V_{OC} and light intensity. Usually, V_{OC} and the natural logarithm of I are related by $V_{OC} \propto n(kT/q)\ln(I)$, where k, T, and q represent the Boltzmann constant, temperature in Kelvin, and elementary charge, respectively. The value of n ranges from 1 to 2, and n equal to unity indicates trap-free conditions. Any deviation from 1 indicates that charge-carrier traps exist to a certain degree in the active layer or the interface between the active layer and the electrode in the device. The fitted α and n values of optimized devices are shown in **Table S10**.

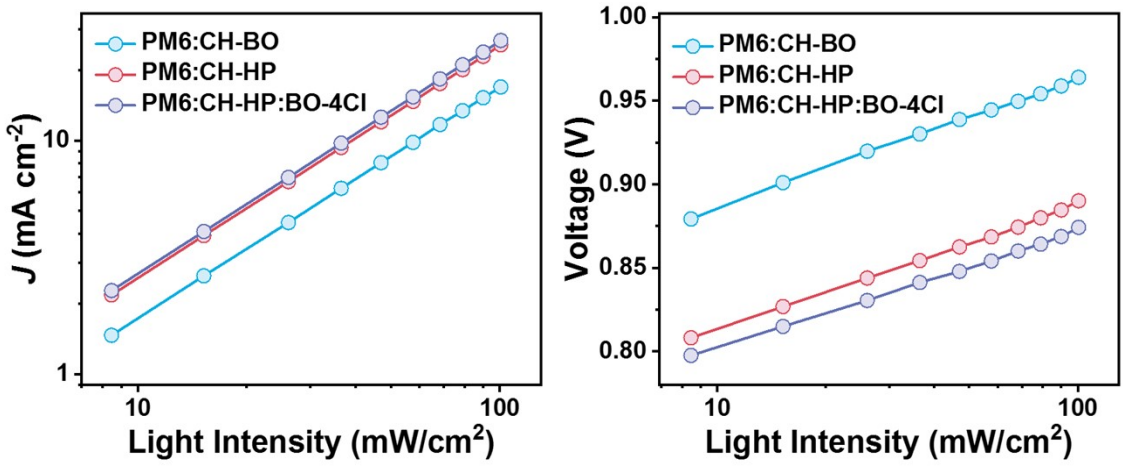

Figure S13. (a) J_{SC} and (b) V_{OC} *vs.* light intensity for optimized for optimized device.

Table S10. The fitted α and n values of optimized devices.

Blend	α	*n*
PM6:CH-BO	**0.991**	**1.29**
PM:CH-HP	0.996	1.26
PM6:CH-HP:BO-4Cl	1.000	1.18

15. Transient photocurrent/photovoltage (TPC/TPV) Characterization

Transient photocurrent (TPC) and photovoltage (TPV) measurements were performed on a Molex 180081-4320 with light intensity about 0.5 sun, Voltage and current dynamics were recorded on a digital oscilloscope (Tektronix MDO4104C). Voltages at open circuit and currents under short circuit conditions were measured over a 1 MΩ and a 50 Ω resistor, respectively.

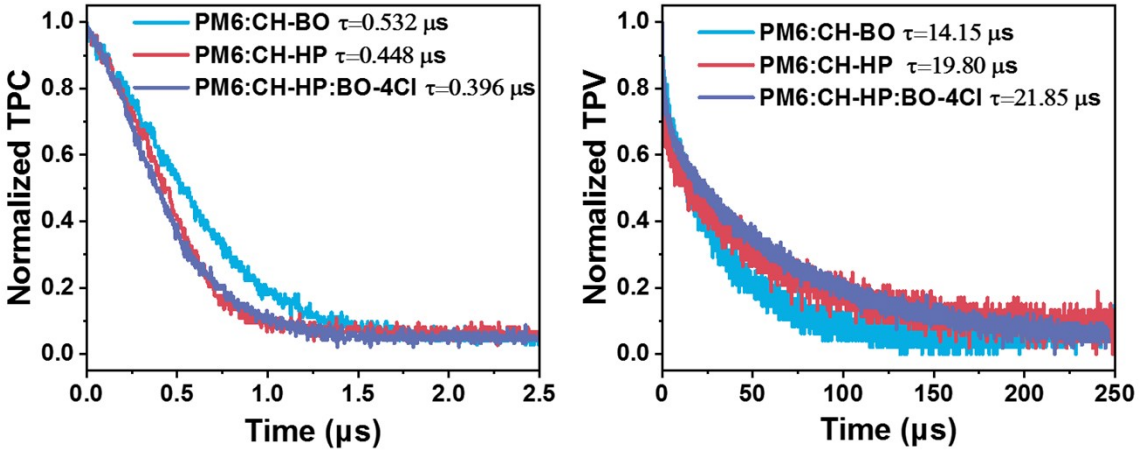

Figure S14. TPC and TPV diagram of optimized OSC devices.

16. Relative Dielectric Constant (ε_r) Test

The dielectric constant should be calculated in terms of the material's geometric capacitance, which represents the capacitance derived from only the material itself (the electronic, atomic, and ionic polarization). The capacitance-frequency of CH-BO and CH-HP based neat films and blended film with PM6 were evaluated with a capacitor architecture of ITO/active layer/Ag at difference frequency from 100 Hz to 1M Hz using Zennium-E under dark conditions and analyzed with the Zahner Analysis software. Between 10^4 Hz and 2×10^5 Hz, a flat capacitive response with respect to frequency is obtained. Then the relative dielectric constant (ε_r) can be calculated according to the equation below:

$$\varepsilon_r = \frac{C_p \times D}{A \times \varepsilon_0}$$

Where C_p is the measured capacitance; D is the thickness of the film; A is the contact area and ε_0 is the permittivity of free space.

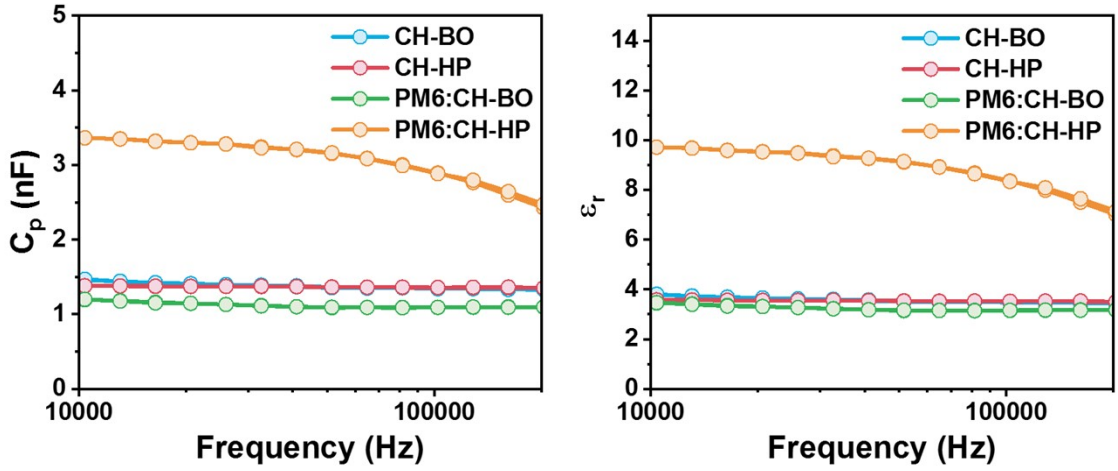

Figure S15. Flat C_p and ε_r response of neat films and blended films at different frequency.

Table S11. Capacitance (C), film thickness (D), device area (A) and dielectric constant at 2×10^5 Hz of neat films and blended films

Film	C (10^{-9} F)	D (mm)	A (mm^2)	εmax r	εavg. r
CH-BO	1.33±0.06	94	4.10	3.54	3.45±0.09
CH-HP	1.35±0.06	94	4.10	3.65	3.49±0.16
PM6:CH-BO	1.10±0.03	105	4.10	3.25	3.17±0.08
PM6:CH-HP	2.43±0.03	105	4.10	7.13	7.04±0.09

17. Atomic Force Microscopy (AFM)

The topographic images of the films were obtained from a Bruker Dimension Icon atomic force microscope using in tapping mode.

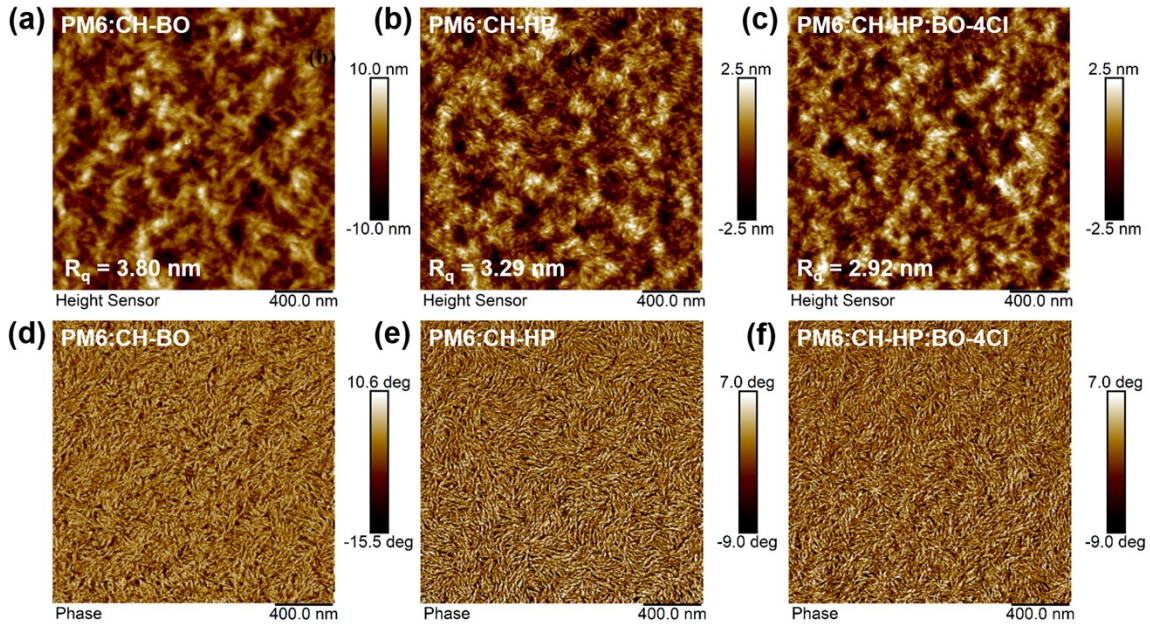

Figure S16. Flat C_p and ε_r response of neat films and blended films at different frequency.

18. Grazing-Incidence Wide-Angle X-ray Scattering (GIWAXS)

GIWAXS measurements were conducted at a Xeuss SAXS/WAXS laboratory beamline. Si substrates were sonicated for 15 min in turn in successive baths of acetone and isopropanol. The substrates were then dried with pressurized nitrogen before being exposed to the UV-ozone plasma for 15 min. Then the samples were prepared by following methods described in Section 8 “Device Fabrication and Characterizations”.

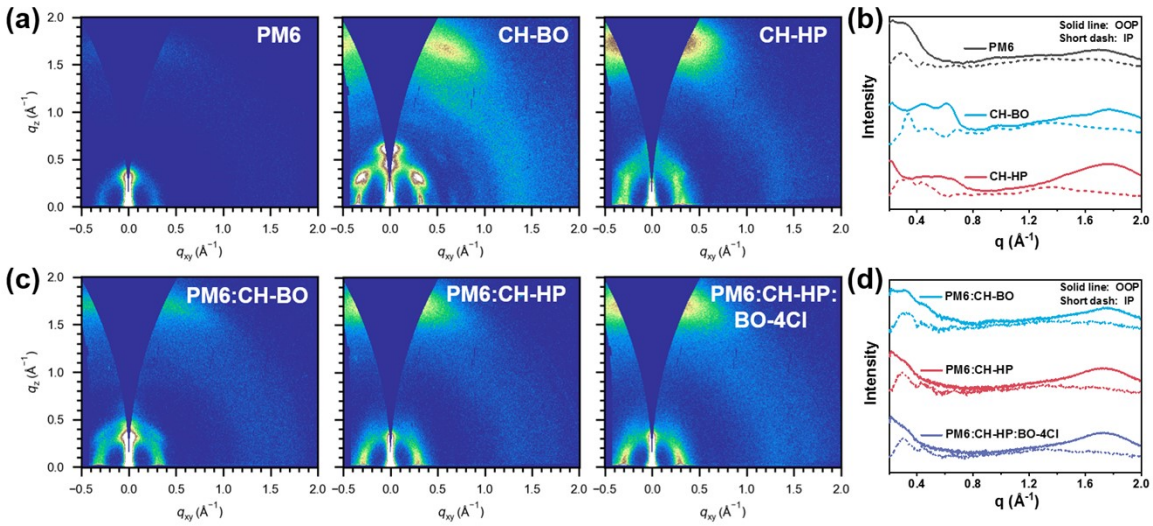

Figure S17. (a, b) 2D GIWAXS patterns and line-cuts of neat films. (c, d) 2D GIWAXS patterns and line-cuts of blend films.

Table S12. Crystallographic parameters of GIWAXS scattering profiles of neat films.

Materials	Lattice plane	Peak location($Å^{-1}$)	d-spacing(Å)	FWHM($Å^{-1}$)	CL(Å)
PM6	100 (IP)	0.291	21.6	0.109	51.9
	010 (OOP)	1.678	3.74	0.430	13.2
CH-BO	100 (IP)	0.337	18.6	0.051	110.9
	010 (OOP)	1.774	3.54	0.367	15.4
CH-HP	100 (IP)	-	-	-	-
	010 (OOP)	1.746	3.60	0.396	14.3

Table S13. Crystallographic parameters of GIWAXS scattering profiles of blend films.

BHJ	Lattice plane	Peak location($Å^{-1}$)	d-spacing(Å)	FWHM($Å^{-1}$)	CL(Å)
PM6:CH-BO	100(IP)	0.319	19.7	0.116	48.7
	010(OOP)	1.736	3.62	0.348	16.2
PM6:CH-HP	100(IP)	0.297	21.2	0.093	60.8
	010(OOP)	1.721	3.65	0.346	16.3
PM6:CH-HP:BO-4Cl	100(IP)	0.303	20.7	0.096	58.9
	010(OOP)	1.722	3.65	0.339	16.7

19. DFT Calculations and MD Simulations

DFT calculation

To calculate the intramolecular charge transfer integrals within the crystal, we have extracted two types of dimers: one type is from two closely stacked NFA molecules within one-dimensional stacking, and the other type is from the two closest molecules between two one-dimensional stacking lines. The wavefunction for these was obtained solely at the PBE0/def2-SVP level using the Gaussian16 software. Subsequently, the charge transfer integral calculations were performed using the program available at https://github.com/snljty/charge_transfer_integral.

MD Force field parameter optimization

The MD simulations of the BHJ of PM6 and CH-BQ/CH-iBQ/CH-BBQ/Y6 were performed in Gromacs 2023 package.[4] The GAFF2 force field was used as initial parameters. The equilibrium bond lengths and angles were updated based on optimized geometries using ztop program. The atomic partial charges were calculated at the PBE0/def2SVP level of theory, and fitted using the restrained electrostatic potential (RESP) method by Multiwfn.[5] The dihedral potentials that dictate the planarity of the conjugated molecules were fitted to the PBE0-D3BJ/def2SVP potential energy surfaces using ztop program.

MD system build and simulation

For PM6/CH-BO and PM6/CH-HP systems, 90 acceptor molecules and 15 chains of PM6 octamers were used for all four systems. The BHJ blends were constructed using the following procedure. First, the molecules were randomly placed into a cubic box with an edge length of 25 nm using packmol software. Then, the NPT run was performed for 20 ns with 10 annealing cycle between 500 K and 300 K to compress the structures. The system was further equilibrated at 300 K for a 10 ns NPT run. Lastly, the production NPT run was performed at 300 K for 12 ns to obtain the trajectories. All the MD simulations employed velocity-Verlet integrator at 2.0 fs time step with LINCS algorithm to constrain bonds with hydrogen. The temperature was controlled with V-rescale thermostat. And pressure was controlled using C-rescale barostat. Five independent simulations were

performed for each system. And the analysis was performed on the frames extracted from the last 10 ns production run with 200 ps interval.

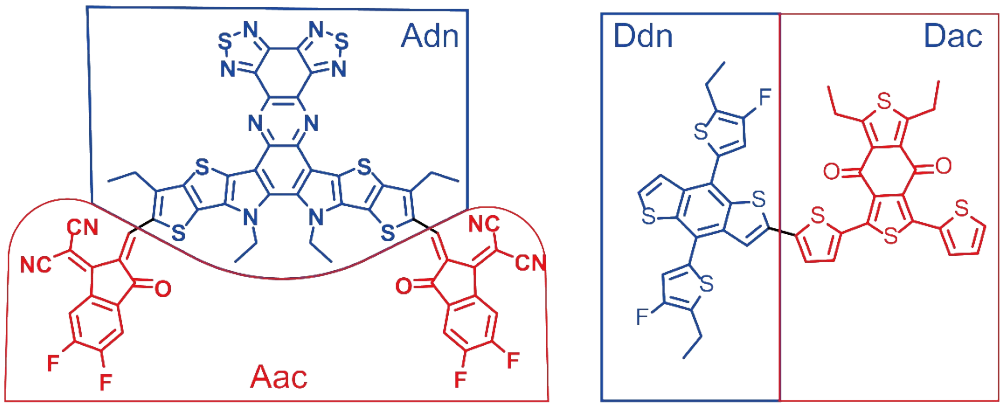

Figure S18. The definition of various fragments from donor/acceptor molecule.

Stacking topology analysis

π-π stacking interactions are critical to electronic activity processes including charge separation, recombination, and the transport of holes and electrons. To investigate these interactions, we performed a stacking analysis on the MD system using the following method: Initially, a criteria was established where non-hydrogen atoms within two conjugated fragments situated at a distance of 3.6 Angstroms or less are considered a close contact. If there are more than two such contacts between two fragments, it is indicative of stacking interactions between them. We identified other fragments that stack with each acceptor group on each acceptor molecule, and then quantified the number of segments with varying neighboring stacking fragments. This was conducted for a total of 5 trajectories, with 50 frames spanning 10 nanoseconds for each trajectory. The mean values and standard deviations obtained are presented in **Table S14**. The notation 'DnAn' denotes that the acceptor segment stacks with 'n' donor and 'n' acceptor molecules.

Table S14. Average number and standard deviation of acceptor molecules in various stacking environments

Stacking env	CH-BO mean	CH-BO std	CH-HP mean	CH-HP std
D0A0	1.2	0.5	1.3	0.6
D0A1	3.3	1.5	2.1	1.2
D0A2	9.7	2.9	5.6	2.0
D0A3	11.2	2.6	7.9	2.4
D0A4	7.6	3.0	4.1	2.0
D0A5	2.3	1.1	1.6	0.8
D0A6	1.3	0.5	1.4	0.6
D0A7	0.1	0.3	1.0	0.2
D0A8	0.0	0.0	0.1	0.3
D0A9	0.0	0.0	0.1	0.2
D1A0	3.1	1.4	1.8	0.9
D1A1	8.2	2.3	9.0	2.8
D1A2	11.5	3.2	11.5	2.9
D1A3	6.3	2.2	9.8	2.2
D1A4	1.8	0.8	2.8	1.7
D1A5	1.4	0.7	1.5	0.7
D1A6	0.6	0.5	1.1	0.3
D1A7	0.0	0.0	0.1	0.3
D1A9	0.0	0.0	0.1	0.2
D2A0	4.4	1.5	2.7	1.3
D2A1	8.1	2.9	9.2	2.4
D2A2	5.1	2.0	8.6	2.7
D2A3	2.2	1.2	4.8	2.2
D2A4	1.1	0.3	2.0	1.0
D2A5	1.1	0.2	1.0	0.2
D2A6	0.0	0.0	0.1	0.3
D2A7	0.0	0.0	0.1	0.2
D3A0	2.0	1.0	1.8	0.7
D3A1	1.9	1.1	2.5	1.3
D3A2	1.8	1.0	1.8	0.9
D3A3	1.1	0.3	1.1	0.3
D3A4	0.1	0.3	1.0	0.0
D3A5	0.0	0.0	0.1	0.3
D4A0	1.0	0.2	1.1	0.2
D4A1	1.0	0.0	1.1	0.3
D4A2	1.0	0.3	1.1	0.3
D4A3	0.1	0.3	0.5	0.5
D5A1	0.1	0.3	0.2	0.4
D5A2	0.3	0.5	0.0	0.0
D6A2	0.1	0.2	0.0	0.0

For each stacking case, we also quantified the number of close contacts between the acceptor segments and the donor-acceptor segments within the donors, as well as the donor-acceptor segments within the acceptors. The results are tabulated in **Table S14 and S15**.

Table S15. Average number of close contacts between acceptor molecules and other conjugated fragments in various stacking environments (part.1).

	CH-BO				CH-HP			
	Dac	**Adn**	**Ddn**	**Aac**	**Dac**	**Adn**	**Ddn**	**Aac**
D1A1	4.8	6.9	5.1	5.8	5.8	5.4	5.2	5.7
D1A3	5.0	7.9	4.8	10.2	5.3	9.1	3.9	10.6
D1A4	3.3	9.1	5.2	11.6	4.2	8.9	4.0	15.7
D2A2	7.3	5.5	5.9	6.6	7.8	6.0	6.1	7.9
D3A2	8.5	6.2	6.5	6.4	11.8	6.0	6.0	5.8
D1A2	5.2	6.0	4.4	8.0	5.5	7.3	4.4	8.3
D4A1	7.5	3.3	13.6	4.5	13.0	2.3	9.4	4.4
D2A0	8.7	0.0	6.3	0.0	8.7	0.0	7.1	0.0
D2A1	8.6	6.2	6.3	4.7	7.9	5.4	6.2	5.9
D2A3	5.5	7.1	6.8	9.8	7.2	6.2	5.8	9.8
D1A0	5.7	0.0	5.3	0.0	7.7	0.0	5.7	0.0
D1A5	3.4	8.7	6.4	16.2	4.1	7.0	3.8	21.8
D3A3	14.4	8.4	5.3	8.5	9.2	5.6	4.2	10.5
D4A0	12.6	0.0	9.8	0.0	9.3	0.0	12.2	0.0
D3A1	9.9	3.9	7.4	4.2	10.8	5.1	6.2	5.1
D2A4	5.7	7.8	7.4	10.8	8.8	6.0	6.1	14.1
D3A0	10.1	0.0	9.5	0.0	10.4	0.0	8.4	0.0
D2A5	3.6	8.5	8.1	14.5	12.4	7.7	3.1	14.8
D4A2	6.0	2.7	14.8	3.6	13.4	6.1	4.4	7.9

Table S16. Average number of close contacts between acceptor molecules and other conjugated fragments in various stacking environments (part.2).

	CH-BO				CH-HP			
	Dac	**Adn**	**Ddn**	**Aac**	**Dac**	**Adn**	**Ddn**	**Aac**
D1A6	2.7	11.5	0.7	16.8	3.9	5.0	2.7	28.2
D3A4	4.3	1.3	1.3	10.3	4.4	6.9	5.3	15.8
D4A3	7.3	0.0	6.7	8.0	11.1	4.7	3.1	8.5
D5A2	7.0	3.6	16.2	2.2	0.0	0.0	0.0	0.0
D5A1	5.0	2.0	13.3	0.0	15.5	0.0	9.8	4.0
D6A2	2.5	0.5	5.8	0.5	0.0	0.0	0.0	0.0
D0A4	0.0	10.4	0.0	14.2	0.0	10.0	0.0	16.0
D0A3	0.0	9.5	0.0	12.4	0.0	9.2	0.0	11.9
D0A2	0.0	8.5	0.0	9.7	0.0	8.0	0.0	8.2
D0A1	0.0	7.7	0.0	7.7	0.0	5.1	0.0	7.3
D0A5	0.0	9.6	0.0	18.4	0.0	11.9	0.0	17.4
D0A6	0.0	10.0	0.0	21.8	0.0	12.5	0.0	21.4
D0A7	0.0	30.0	0.0	11.0	0.0	13.9	0.0	22.1
D0A8	0.0	0.0	0.0	0.0	0.0	4.0	0.0	31.0
D0A9	0.0	0.0	0.0	0.0	0.0	3.0	0.0	15.5
D1A9	0.0	0.0	0.0	0.0	0.0	3.3	0.7	11.3
D1A7	0.0	0.0	0.0	0.0	1.5	7.0	1.0	8.5
D2A7	0.0	0.0	0.0	0.0	1.3	4.8	0.5	3.3
D2A6	0.0	0.0	0.0	0.0	2.8	3.8	0.5	9.8
D3A5	0.0	0.0	0.0	0.0	3.0	0.0	6.0	19.0

Acceptor types from **Tables S14-S16** were further categorized and summarized to produce **Figures 6d** and **6e** in the manuscript. Based on **Tables S14-S16**, we generated stacking topology graphs using the networkx library in Python. For clarity in presentation, the polymer donor was simplified from fifteen octamers to five 24-mers, meaning five nodes represent the donor molecules. This simplification is valid because there is a sufficient number of close contacts between the donor molecules, and the degree of polymerization typically used in experiments is around 25, which is higher than that used

in the simulations. Consequently, the stacking of the donor molecules is usually ample and was not specifically investigated in this study. Then, for the 90 NFA molecules in the system, we connected them with varying numbers of polymer and NFA molecules based on the stacking information of the different types of acceptor molecules as reported in **Table S15**. The weight of the connections, or edges, was calculated based on the number of close contacts listed in **Table S16** and **S17**. The associated Python script, "bulkgraph.py," has been published in https://gitee.com/coordmagic/bulkgraph.

Stacking topology analysis

We also conducted an analysis of the neighboring atom composition for different fragments as follows: For conjugated segments, we selected non-hydrogen atoms within 3.6 angstroms of the central segment non-hydrogen atom, or hydrogen atoms within 3.0 angstroms, and defined them as neighbor atoms. For alkyl chains, we chose non-hydrogen atoms from other fragments within 3.0 angstroms of their hydrogen atoms or other hydrogen atoms within 2.4 angstroms, defining them as neighboring atoms. Then, for each type of central fragment, we analyzed the average composition of its neighbor atoms. This allows us to determine the proportion of other functional groups surrounding a group, thereby gaining insight into the average interactions between various types of functional groups. The results are shown in **Table S17-S19**.

Table S17. Average number and standard deviation of neighboring atoms from various fragments around each Aac segment.

Group	CBO		CHP	
	mean	std	mean	std
Aac	3.7	0.5	3.9	0.6
And	2.3	0.2	2.3	0.2
Ddn	1.3	0.1	1.5	0.2
Dac	1.6	0.2	2.1	0.3
AR-side (self)	4.1	0.1	3.3	0.1
AR-core (self)	1.2	0.1	1.2	0.1
AR-side (other)	2.9	0.2	1.8	0.2
AR-core (other)	3.7	0.3	3.9	0.2
DR	4.1	0.3	4.8	0.4
Aryl-H	0.6	0.1	0.7	0.1

Table S18. Average number and standard deviation of neighboring atoms from fragments surrounding each AR-side segment (single BO or HP alkyl chain).

Group	CBO		CHP	
	mean	std	mean	std
Aac	2.0	0.1	1.6	0.1
And	4.1	0.1	3.8	0.0
Ddn	2.0	0.1	1.3	0.2
Dac	1.1	0.1	0.7	0.1
AR-side (self)	1.0	0.1	0.7	0.1
AR-core (self)	1.0	0.1	0.8	0.1
AR-side (other)	3.2	0.2	2.0	0.2
AR-core (other)	2.2	0.1	1.6	0.1
DR	1.3	0.0	1.2	0.0
Aryl-H	2.0	0.1	1.6	0.1

Table S19. Average number and standard deviation of neighbor atoms from different fragments around each Adn segment.

Group	CBO		CHP	
	mean	std	mean	std
Aac	4.0	0.4	4.0	0.3
And	2.9	0.3	3.6	0.5
Ddn	1.2	0.3	1.7	0.2
Dac	1.3	0.3	1.7	0.2
AR-side (self)	15.9	0.2	13.1	0.1
AR-core (self)	18.0	0.2	18.0	0.2
AR-side (other)	2.4	0.3	1.6	0.2
AR-core (other)	3.2	0.2	3.2	0.2
DR	3.7	0.2	4.5	0.4
Aryl-H	0.5	0.1	0.7	0.1

20. Solution NMR Spectra

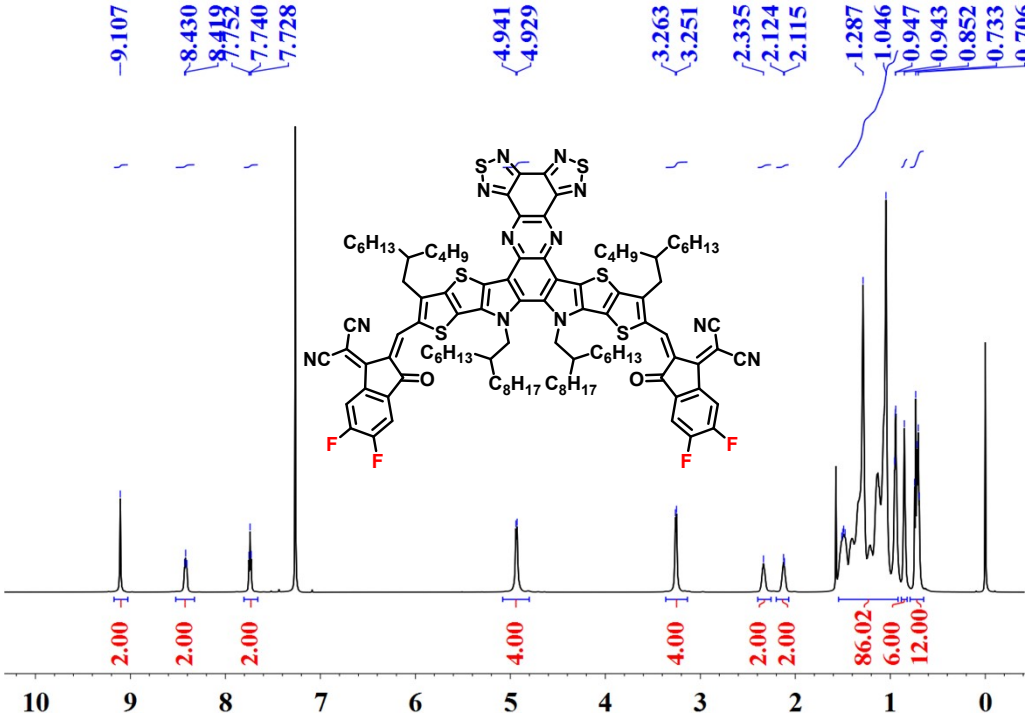

Figure S19. ^{1}H NMR spectrum of **CH-BO** in $CDCl_3$

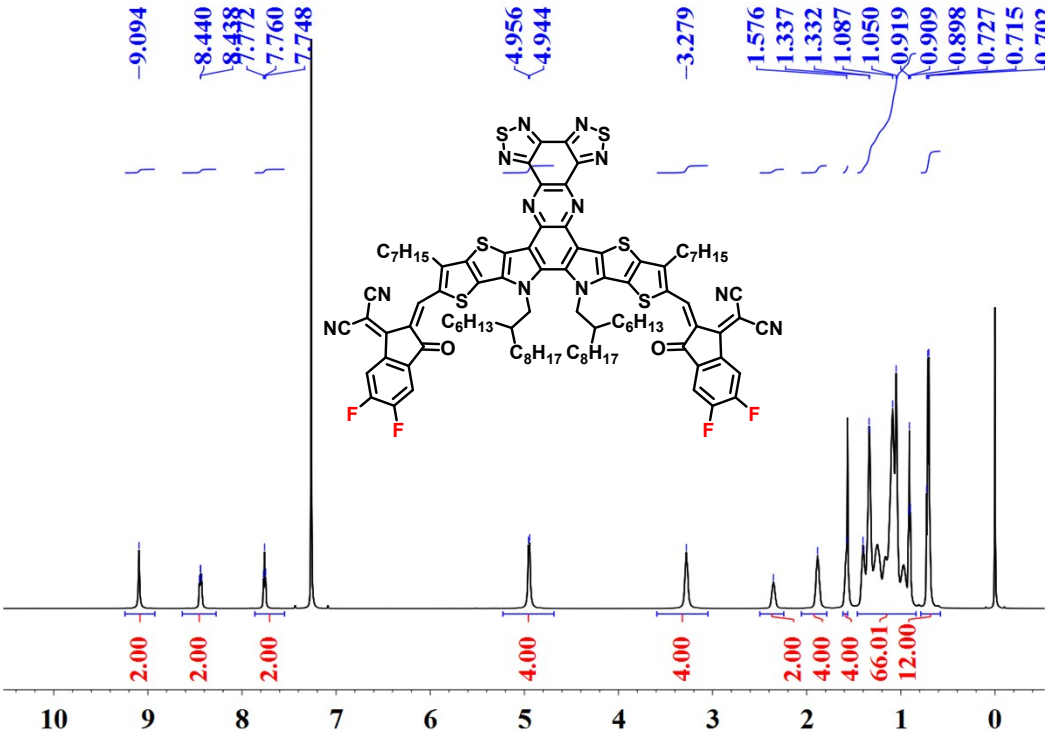

Figure S20. ^{1}H NMR spectrum of **CH-HP** in $CDCl_3$

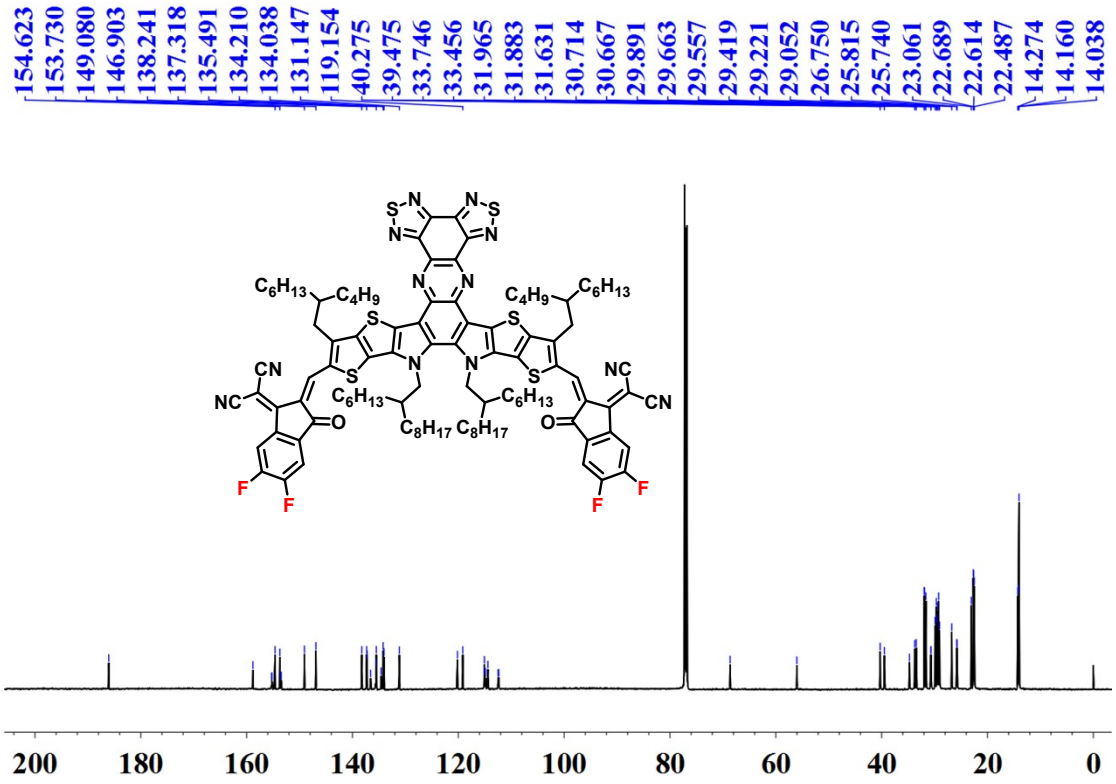

Figure S21. ^{13}C NMR spectrum of **CH-BO** in $CDCl_3$

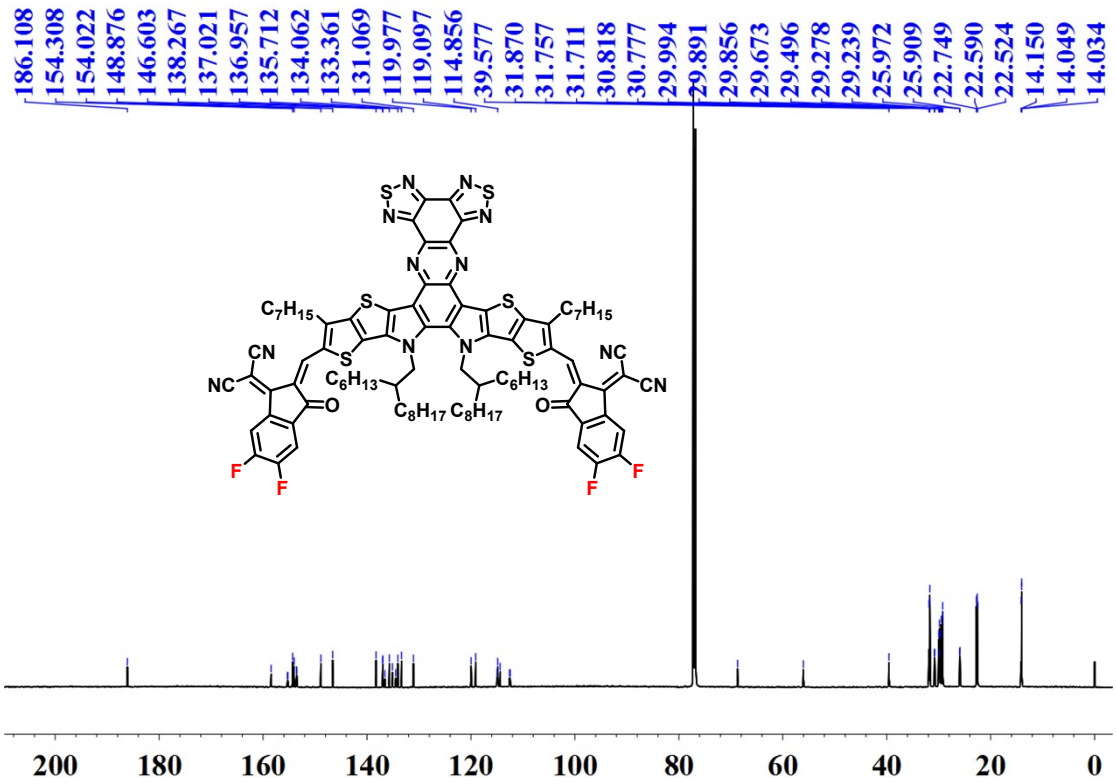

Figure S22. ^{13}C NMR spectrum of **CH-HP** in $CDCl_3$

21. High-Resolution Mass Spectra

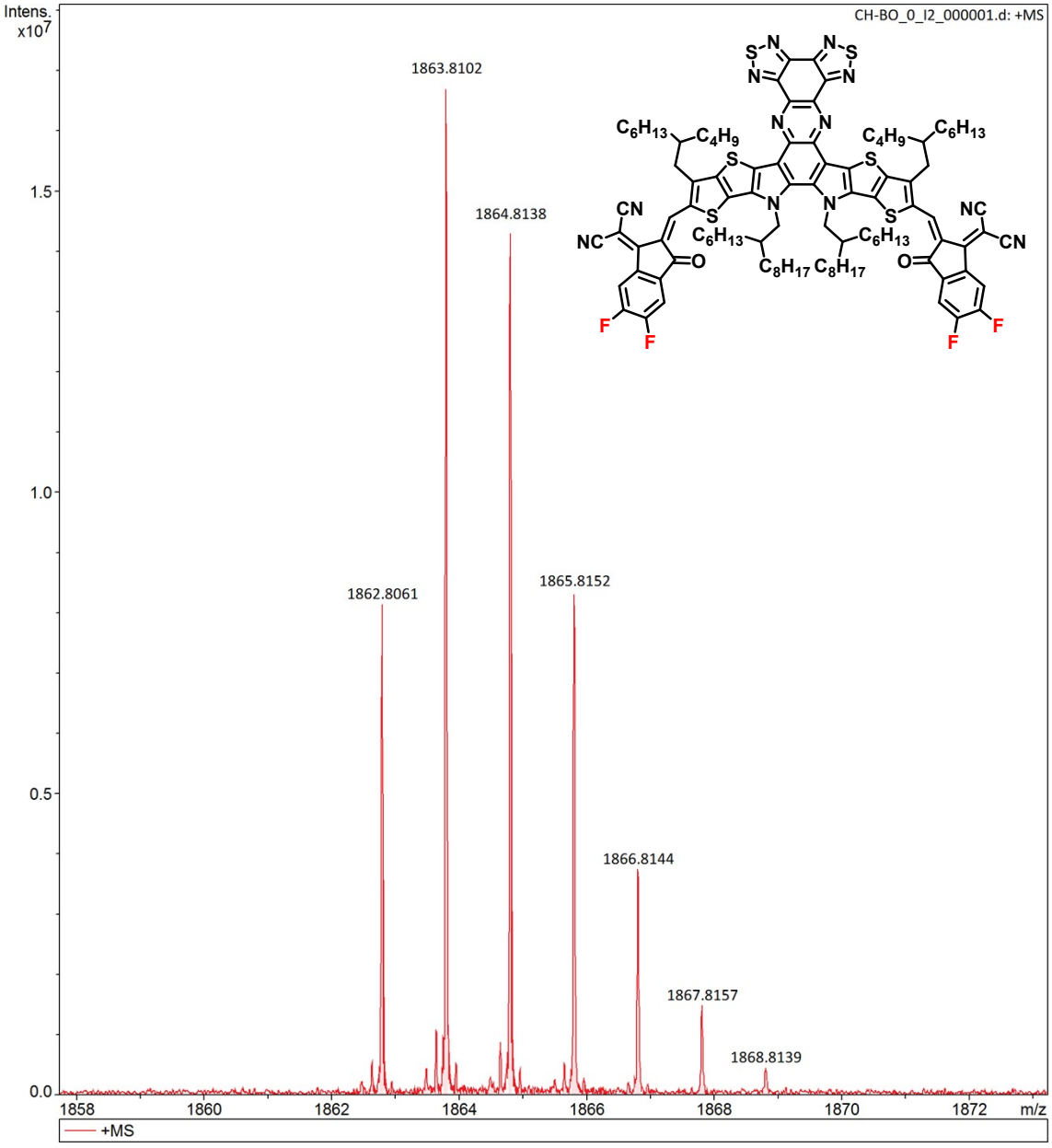

Figure S23. HR-MS spectrum of **CH-BO**

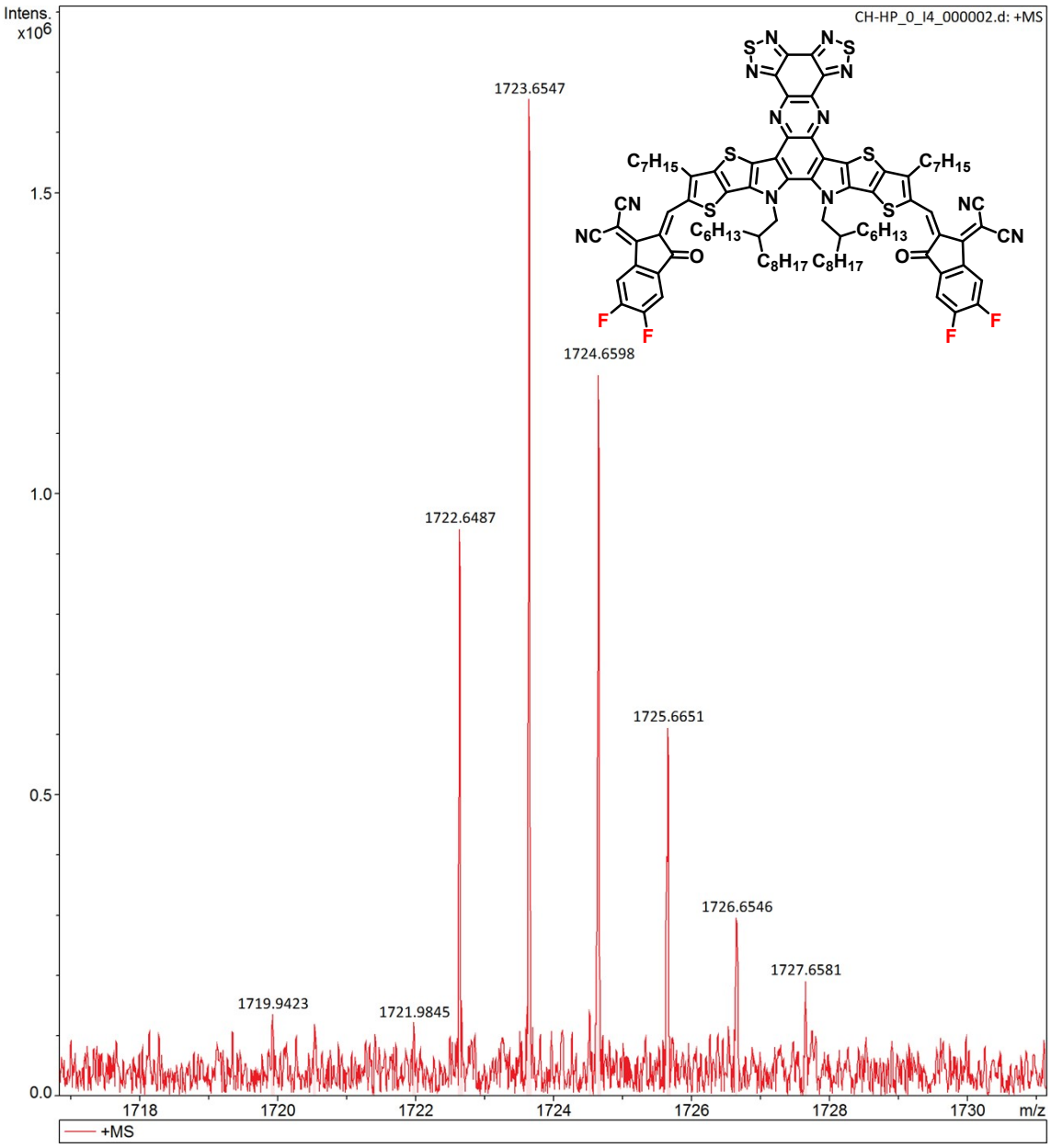

Figure S24. HR-MS spectrum of **CH-HP**.

22. Supplementary References

[1] Duan T, *et al.* Electronic Configuration Tuning of Centrally Extended Non-Fullerene Acceptors Enabling Organic Solar Cells with Efficiency Approaching 19%. *Angew. Chem. Int. Ed.* **62**, e202308832 (2023).

[2] Pommerehne Jörn, *et al.* Efficient two layer leds on a polymer blend basis. *Adv. Mater.* **7**, 551–554 (1995).

[3] Wu Z, *et al*. n-Type Water/Alcohol-Soluble Naphthalene Diimide-Based Conjugated Polymers for High-Performance Polymer Solar Cells. *J. Am. Chem. Soc.* **138***,* 2004–2013 (2016).

[4] Abraham M J, *et al.* GROMACS: High performance molecular simulations through multi-level parallelism from laptops to supercomputers. *SoftwareX* **1–2***,* 19–25 (2015).

[5] Lu T, et al. Multiwfn: A Multifunctional Wavefunction Analyzer. *J. Comput. Chem.* **33**, 580–592 (2012).